Signal-to-noise analysis of biomedical photoacoustic measurements in time and frequency domains

Sergey Telenkov and Andreas Mandelis
Center for Advanced Diffusion Wave Technologies (CADIFT), Department of Mechanical and Industrial Engineering, University of Toronto, Toronto, Ontario, M5S 3G8 Canada

(Received 23 June 2010; accepted 4 October 2010; published online 13 December 2010)

Sensitivity analysis of photoacoustic measurements is conducted using estimates of the signal-to-noise ratio (SNR) achieved under two different modes of optical excitation. The standard pulsed time-domain photoacoustic imaging is compared to the frequency-domain counterpart with a modulated optical source. The feasibility of high-SNR continuous wave depth-resolved photoacoustics with frequency-swept (chirp) modulation pattern has been demonstrated. Utilization of chirped modulation waveforms achieves dramatic SNR increase of the periodic signals and preserves axial resolution comparable to the time-domain method. Estimates of the signal-to-noise ratio were obtained using typical parameters of piezoelectric transducers and optical properties of tissue. © *2010 American Institute of Physics*. [doi:10.1063/1.3505113]

I. INTRODUCTION

Biomedical photoacoustics has made significant progress in recent years and has approached the stage when clinical imaging instrumentation utilizing photoacoustic (PA) principles may become available in the near future. Rapid development of PA imaging has been motivated by its potential superior diagnostic capabilities unavailable through other means such as conventional ultrasound. Several research projects are aimed at the early detection of breast cancer and currently are at an advanced preclinical stage.[1,2] Addition of multiwavelength optical sources to the conventional PA modality provides promising development toward molecular and spectroscopic imaging.[3–6] All these and other imaging applications rely exclusively on short-time (nanosecond) laser exposure and detection of broadband pressure transients generated in subsurface tissue chromophores. One of the drawbacks that may affect clinical adoption of PA technology, however, is the need for bulky and relatively expensive Q-switched nanosecond laser systems with an optional optical parametric oscillator for wavelength tuning. In addition to the size and cost, such systems require trained personnel for regular maintenance and controlled stable environment for consistent operational characteristics. The prospect of using inexpensive and compact optical sources for PA imaging applications would be a real breakthrough in the development of commercially successful PA instrumentation. In the past few years, we actively developed an alternative approach to PA imaging using an intensity-modulated near-IR continuous wave (CW) laser source, which may eventually become a prototype for a portable instrument suitable for clinical applications. The obvious drawback of a PA system based on a CW laser source is the limited optical power that can be delivered to the imaged tissue chromophores and, as a result, very weak acoustic pressure waves are generated. Detection of the weak acoustic signals and image reconstruction demand particular attention to be paid to the sensitivity of ultrasonic transducers, noise level in the system, and the signal processing algorithm, which is used to obtain spatially resolved information. In our treatment of PA imaging with a CW optical source we follow the principles utilized for decades by radar and sonar technologies historically used in attempts to increase the detection range with limited power transmitters without compromising the axial resolution. In this paper, we analyze two photoacoustic modalities with respect to signal-to-noise ratio (SNR) and their ability to image optical heterogeneities hidden in light-scattering media. We show that SNR of CW photoacoustics can be increased several orders of magnitude by utilizing frequency-swept modulation waveforms and correlation signal processing. Estimates of the photoacoustic pressure were obtained using a simplified one-dimensional model of a chromophore layer immersed in light-scattering media with optical properties similar to human tissue. Typical values of commercial piezoelectric transducer sensitivity and bandwidth are used to estimate the signal magnitude and the noise level. Particular attention is given to PA signals with linear frequency modulation and the application of correlation processing for signal compression to improve SNR and axial resolution.

II. PULSED TIME-DOMAIN PHOTOACOUSTICS

Biomedical photoacoustic imaging allows visualization of optical heterogeneities inside the targeted tissues with resolution compared to conventional ultrasound imaging. The strong optical scattering of human tissues represents major difficulty and limitation for PA imaging of deep tissue chromophores. Since optical irradiance incident upon tissue must be limited for safety reasons, the photogenerated acoustic pressure will be limited as well. Therefore the system noise floor will ultimately define the achieved maximum imaging depth and the minimal optical contrast that can be resolved with PA imaging. Analytical treatment of the photoacoustic effect with pulse duration $t_L < 10$ ns ignores heat conduction, and laser-induced pressure is governed by the wave equation which is for one-dimensional case

$$\left[\frac{\partial^2}{\partial z^2} - \frac{1}{c_a^2}\frac{\partial^2}{\partial t^2}\right] p(z,t) = \frac{-\beta}{C_p}\frac{\partial q(z,t)}{\partial t},$$

where c_a is the speed of sound, β is the thermal expansion coefficient, C_p is the specific heat capacity, and the source function $q(z,t)$ is the absorbed energy per unit of time and volume. For the purpose of numerical estimates, we consider here a simplified one-dimensional model of acoustic wave generation that can be applied to a light-absorbing layer immersed in optically scattering medium. Since heat conduction is neglected at the short time scale, the source function $q(z,t)$ is determined by the light distribution in the targeted tissue. Assuming uniform optical irradiance of the tissue surface I_0 (W/cm^2), attenuation of diffuse light can be described approximately by Beer's law:

$$I(z) = I_0 \exp(-\mu_{\text{eff}} z), \tag{1}$$

where μ_{eff} is the tissue effective attenuation coefficient. For human tissues μ_{eff} depends strongly on the wavelength and the type of tissues.[7] For our estimates, we assume that scattering dominates in tissues with the reduced scattering coefficient $\mu_s' = 10$ cm^{-1} and the absorption coefficient $\mu_a \ll \mu_s'$, giving for surrounding media $\mu_{\text{eff}} = [3\mu_a(\mu_a + \mu_s')]^{1/2} \sim 1.5$ cm^{-1}. In the case of instantaneous heating, laser temporal profile can be approximated by the delta-function and the peak acoustic pressure p_0 excited in a chromophore with absorption coefficient μ_a positioned at depth z_0 is

$$p_0 = \frac{c_a^2 \beta \mu_a E}{2C_p} = \frac{c_a^2 \beta \mu_a E_0}{2C_p} \exp(-\mu_{\text{eff}} z_0), \tag{2}$$

where E_0 is the incident optical energy per unit of surface area. Depending on the boundary conditions at the chromophore interface, the acoustic signals will be unipolar or bipolar pressure transients with characteristic duration $(\mu_a c_a)^{-1}$ propagating in both directions.[8] We can neglect acoustic attenuation for acoustic waves whose spectrum is limited to 1–5 MHz, which is usually the case for weakly absorbing macroscopic tissue chromophores. For estimation of peak characteristics, we do not need to know the exact shape of the detected signal, which is given by a convolution of the transducer impulse response and the temporal profile of the acoustic pressure. In time-domain measurements, the transducer bandwidth is normally greater than the acoustic response spectrum to avoid signal distortions and possible artifacts in image reconstruction.[9] Therefore, to evaluate the peak magnitude of the detected signal we simply take the transducer sensitivity ξ as a constant. The exact value of ξ varies for different types of transducers and must be determined from calibration measurements. Several authors[10,11] conducted such measurements and cited typical values of sensitivity of polymer film transducers at $\xi = 6$–10 μV/Pa. Using these values, we can estimate the peak voltage signal as

$$V_0 = \xi p_0 = \xi \frac{c_a^2 \beta \mu_a E_0}{2C_p} \exp(-\mu_{\text{eff}} z_0). \tag{3}$$

The safety standard[12] regulates the optical exposure level through a parameter called maximum permissible exposure (MPE) in units of joules per square centimeter. Thus for laser pulses of duration 10 ns and wavelength 1064 nm, the MPE is equal to

$$E_{\text{MPE}} = 0.1\ \text{J/cm}^2. \tag{4}$$

Adopting the transducer sensitivity $\xi = 6$ μV/Pa, $E_0 = E_{\text{MPE}}$, and typical material parameters $c_a = 1.5 \times 10^5$ cm/s, $\beta = 2 \times 10^{-4}$ K^{-1}, $C_p = 4.2 \times 10^3$ J/(kg K), and $\mu_{\text{eff}} = 1.5$ cm^{-1}, we can express the peak voltage as a function of two parameters: the chromophore absorption coefficient μ_a (cm^{-1}) and its depth z_0 (cm):

$$V_0(z_0, \mu_a) = 3.4 \times 10^{-2} \mu_a \exp(-1.5 z_0). \tag{5}$$

Equation (5) can be used for numerical estimates of the peak signal voltage. For example, a chromophore layer with $\mu_a = 2$ cm^{-1} positioned at the depth of 3 cm is expected to generate an acoustic pressure response that can produce peak voltage of $\sim$750 μV. To estimate the signal-to-noise ratio we employ the standard definition as a ratio of the signal power to the mean power of the noise signal present in the detection channel:

$$\text{SNR} = \frac{P_s}{P_N} = \frac{V_0^2}{\langle V_N^2 \rangle}, \tag{6}$$

where $\langle V_N^2 \rangle$ is the noise mean square voltage. For thermal noise it is given by the Nyquist equation $\langle V_N^2 \rangle = 4k_B T R \Delta f$, where k_B is the Boltzmann constant, T is the absolute temperature, R is the load resistor, and Δf is the detection bandwidth. The absolute value of $\langle V_N^2 \rangle$ depends on the transducer electric characteristics such as capacitance and the frequency bandwidth. Since accurate detection of short acoustic transients requires wide frequency bandwidth, this inevitably results in high noise background. In practice, optimal transducer bandwidth is selected by balancing acceptable noise level and the maximum acoustic frequency needed for adequate spatial resolution. According to data available in the literature,[11,13] a polymer film transducer with sensitivity $\xi = 6$ μV/Pa and bandwidth $\sim$2 MHz has thermal noise level approximately 40 μV. If we use this value as a thermal noise limit, then the SNR of a time-domain measurement for a chromophore layer positioned 3 cm deep will be $\sim$25 dB. Further increase in SNR is possible by averaging multiple signals but it maybe impractical for low repetition rates of a laser source; besides, the maximum number of pulses must be limited due to safety regulations applied to the mean irradiance of an entire pulse train. In addition to the stochastic thermal noise, detection of PA transients must deal with unwanted interference signals stemming from light absorption in surrounding tissues and in transducer itself exposed to the scattered radiation. These factors result in unstable baseline that complicates acoustic signal detection and image reconstruction especially in the back-propagation mode where a single tissue surface is used for laser irradiation and detection. A typical profile of the photoacoustic response from a planar absorber with $\mu_a = 2$ cm^{-1} immersed in a scattering Intralipid solution at the depth of 2 cm is shown in Fig. 1 (arrow). Data were recorded[14] using a focusing transducer with the focal distance of 2.5 cm and the peak frequency response at 3.5 MHz. It must be noticed that the major problem for reliable detection of acoustic signal in back-propagation mode comes from unstable baseline caused by the transducer reverberations following direct laser absorption in the transducer itself and multiple reflections in the transducer housing. Unless the interfering signal is reduced dramatically, it will severely affect the estimated

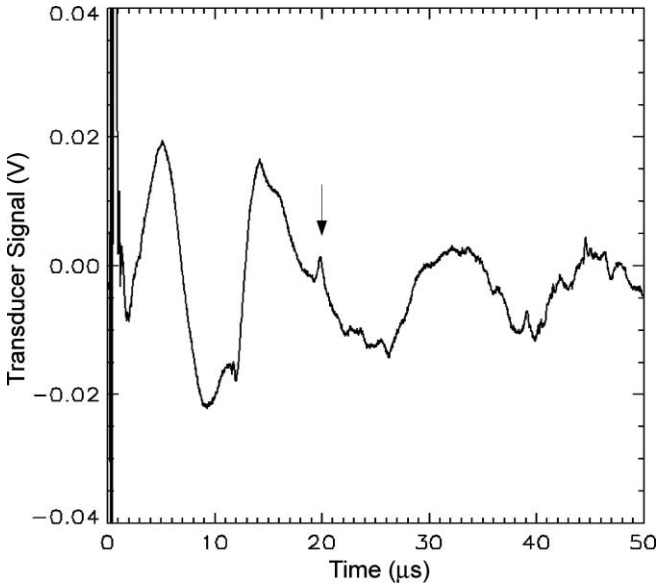

FIG. 1. Voltage signal recorded with a wideband focusing ultrasonic transducer (3.5 MHz) in response to pulsed optical irradiation of a light-scattering phantom. Photoacoustic response of a subsurface chromophore with $\mu_a = 2\ \mathrm{cm}^{-1}$ is indicated with the arrow.

SNR, the maximum imaging depth, and the overall image contrast. Since the baseline signal is not random, it cannot be reduced by simple averaging and some other form of signal conditioning must be used. The standard approach to baseline interference reduction is high-pass filtering, which removes the low frequency components and preserves sharp edges associated with the targeted response. However this method cannot be applied in all situations since signal itself is broad band and its spectrum frequently overlaps with that of interference, especially in the case of weakly absorbing or relatively large chromophores. The filtering procedure can be refined to adapt to specific temporal shape such as in wavelet-based routines[1,13] but this method requires some *a priori* information about the signal profile. The merits of various signal conditioning algorithms are not discussed here, but we demonstrate that signal-to-noise ratio of time-domain measurements is not limited to the thermal noise and image contrast can be much less than the estimated 25 dB. Since the thermal noise is not the only source of noise, Eq. (6) should be modified to take into account all other interfering signals:

$$\mathrm{SNR} = \frac{P_s}{P_N + P_I},$$

where P_I is the interference power, which is highly depended on the specifics of experimental setup. Thus, the estimates based on Eq. (6) give merely high-limit or the best case scenario SNR when all other interfering signals can be neglected.

III. FREQUENCY-DOMAIN PHOTOACOUSTIC IMAGING

It was demonstrated in our previous studies[14–16] that spatially resolved photoacoustic imaging can be realized using a CW laser source with intensity modulation in the megahertz frequency range (0.5–10 MHz). There are two major disadvantages to CW photoacoustics: first, since the mean laser power is limited to 1–10 W, the magnitude of generated acoustic waves is extremely small; second, detection of a narrowband acoustic response cannot provide sufficient spatial resolution required for image formation. To estimate the typical magnitude of acoustic pressure and SNR of frequency-domain photoacoustics, we use the same one-dimensional model and material parameters as in Sec. II. Using properties of Fourier transforms, the one-dimensional wave equation can be written in the form of the Helmholtz equation for the pressure spectrum:

$$\frac{\partial^2 \tilde{p}}{\partial z^2} + k^2 \tilde{p}(z,\omega) = \frac{-i\omega\beta}{C_p}\tilde{q}(z,\omega),$$

where $\tilde{q}(z,\omega)$ is the temporal Fourier transform of the source function and $k = \omega/c_a$ is the absolute value of wave vector. Again, assuming the chromophore position at z_0 inside scattering media, the source function for uniform light absorption is

$$\tilde{q}(z,\omega) = \mu_a I(z_0)\tilde{F}(\omega)\exp\left(-\mu_a|z-z_0|\right), \quad z \geq z_0,$$

where $I(z_0)$ is the laser irradiance at the chromophore position and $\tilde{F}(\omega)$ is the Fourier spectrum of a modulation waveform. Solution of the inhomogeneous Helmholtz equation for a single frequency ω_0 modulation $\tilde{F}(\omega) = 2\pi\delta(\omega-\omega_0)$ can be found considering wave propagating in the direction $z < z_0$ and using stress-free boundary condition. Then applying inverse Fourier transform, the plain pressure wave is

$$p(z,t) = \frac{i\omega\beta\mu_a I(z_0)}{\left(\mu_a^2 + \omega_0^2/c_a^2\right)C_p}\exp\left[i\omega_0\left(t + \frac{|z-z_0|}{c_a}\right)\right].$$

Assuming that optical irradiation at z_0 can be approximated by the Eq. (1), we obtain an estimate for the pressure amplitude in acoustic wave:

$$p_0(\omega) = \frac{\omega\beta\mu_a I_0}{C_p\left(\mu_a^2 + \omega^2/c_a^2\right)}\exp(-\mu_{\mathrm{eff}}z), \tag{7}$$

where I_0 is, as before, the tissue surface irradiance and ω is the angular modulation frequency. Equation (7) follows from a more general formalism[10,17] in the special case of slow heat conduction and ideal acoustic matching interface between the optical heterogeneities and the surrounding media. The acoustic spectrum [Eq. (7)] has a maximum at the characteristic frequency $\omega_a = \mu_a c_a$, which has the physical meaning of matching acoustic wavelength and optical penetration depth. For the power level available from a typical near-IR CW laser source, the amplitude $p_0(\omega)$ is much lower than the thermal noise floor. However, the SNR can be increased several orders of magnitude if we use linear frequency-modulated (chirp) waveforms and apply correlation processing to the received photoacoustic response. The cross-correlation operation, also known as matched filtering in radar signal processing,[18] is expressed using frequency-domain signal representation as

$$B(t-\tau) = \frac{1}{2\pi}\int_{-\infty}^{\infty}\tilde{V}_r^*(\omega)\tilde{V}_0(\omega)e^{i\omega(t-\tau)}d\omega, \tag{8}$$

where $B(t-\tau)$ is the cross-correlation function of the received signal $V_0(t)$ and the modulation reference signal $V_r(t)$. It is

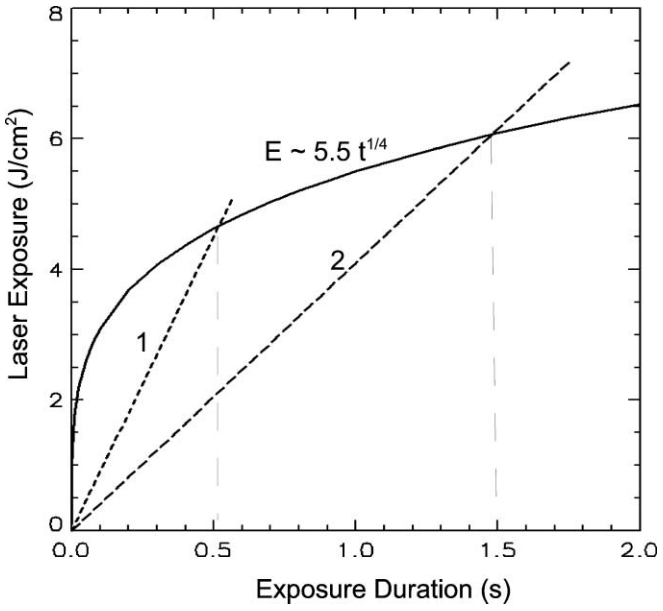

FIG. 2. Maximum permissible exposure of human skin (solid curve) and exposure level as a function of time for two values of optical irradiance $I_0 = 9$ W/cm^2 (line 1) and 4 W/cm^2 (line 2).

clear from Eq. (8) that in the special case of autocorrelation when the received signal is an exact replica of the reference, the magnitude of B at $t = \tau$ is simply the total energy of signal. Use of linear frequency-modulated waveforms with finite bandwidth allows one to implement depth-resolved detection and significantly increase the SNR by correlation processing. In order to estimate the SNR of frequency-domain PA measurements and compare with the time-domain counterpart, we need to look at the safety regulations applicable to relatively long laser exposures. The safety standard[12] sets the maximum exposure level for $\lambda = 1064$ nm and the exposure duration $t = 10^{-7}$–10 s as $E_{\mathrm{MPE}} = 5.5t^{0.25}$ (J/cm^2). Graphically, the safety curve is shown in Fig. 2 (solid line). The area below the solid line is the safety zone for different exposure times. In the coordinate system shown in Fig. 2, the surface irradiance I_0 is merely the slope of a straight line that eventually intersects the safety curve. Two examples of laser irradiance with $I_0 =$ 9 and 4 W/cm^2 are shown as dashed lines that intersect the safety curve, respectively, at the times

$$t_{\max} = \left(\frac{5.5}{I_0}\right)^{4/3} = 0.5 \text{ and } 1.5 \text{ s}. \tag{9}$$

It is interesting to compare the SNR of PA signals before and after correlation processing. Using Eq. (7) we find, for example, that at $I_0 = 9$ W/cm^2 and for the same planar chromophore at 3 cm depth, the acoustic pressure is $p_0 = 3.2 \times 10^{-2}$ Pa and the amplitude voltage is $V_0 = 0.2$ μV for the same value of transducer sensitivity ξ. Assuming the same level of thermal noise as before, the signal-to-noise ratio is

$$\mathrm{SNR}_{\mathrm{in}} = \frac{V_0^2}{2\langle V_{\mathrm{n}}^2\rangle} = 1.25 \times 10^{-5} = -49 \text{ dB}, \tag{10}$$

which makes impossible to measure the signal with standard time-resolved methods. However, correlation processing represented by Eq. (8) coherently adds all frequency components within the signal bandwidth to produce a matched filter output. This operation gives significant increase in SNR. In the case of linear frequency sweep, the SNR gain factor of an ideal matched filter is equal to the time-bandwidth product $m = T_{\mathrm{ch}}\Delta f$, where T_{ch} is the chirp duration and Δf is the bandwidth:

$$\frac{\mathrm{SNR}_{\mathrm{out}}}{\mathrm{SNR}_{\mathrm{in}}} = m. \tag{11}$$

In contrast to conventional ultrasound with chirped waveforms, photoacoustic imaging does not have the round-trip limitation for the chirp duration because the ultrasonic transducer is used only in reception mode and the time-bandwidth product can be quite large. For example, if the chirp central frequency is $f_c = 3$ MHz, the chirp bandwidth can be set at 4 MHz, provided the ultrasonic transducer sensitivity extends up to 5 MHz. Therefore, for the maximum chirp duration of 500 ms derived from the safety limit and 4 MHz bandwidth, the SNR gain due to correlation processing is 2×10^6 and the resulting SNR is

$$\mathrm{SNR}_{\mathrm{out}} \approx 14 \text{ dB}, \tag{12}$$

which makes detection of tissue chromophores positioned as deep as 3 cm below the surface possible. In practice, use of chirps with duration of several hundreds of milliseconds is not convenient from the standpoint of digital data acquisition with high sampling rates. It is more effective to divide the maximum allowed chirp duration into smaller chirps with the same bandwidth and average the resulting signals coherently prior to processing to achieve the same SNR gain. Although the estimated SNR of the frequency-domain method is still lower than the thermal-noise-limited pulsed measurement by approximately 10 dB, the photoacoustic response becomes detectable. The initial long chirped signal is compressed into a narrow correlation peak with the full width less than a microsecond long, which enables imaging with submillimeter axial resolution. In comparison with the time-domain technique, one should bear in mind the high level of baseline interference which significantly reduces the SNR and the resulting image contrast. As shown in Fig. 1, the strong interference signal stimulated by the laser pulse at time $t =$ 0 persists for tens of microseconds, blocking the PA response from the targeted chromophore. On the other hand, in frequency-domain photoacoustics with correlation processing, the effect of an interference coherent with the reference signal is limited to the time $\Delta t = 1/\Delta f$, where Δf is the chirp bandwidth. Since for the bandwidth $\Delta f = 4$ MHz, temporal width of the correlation function $\Delta t < 1$ μs, the effect of strong reverberation launched at $t = 0$ is negligible at times greater than 20 μs, corresponding to PA response arrival. Therefore, SNR of frequency-domain measurements may become comparable to that obtained with time-domain photoacoustics. The additional phase information contained in the complex-valued correlation function may be used to increase image contrast by filtering out the pixels where correlation is observed from the background noise pixels.[16,19] In general, use of chirped waveforms for PA imaging is more versatile since it allows one to tailor the photoacoustic response with

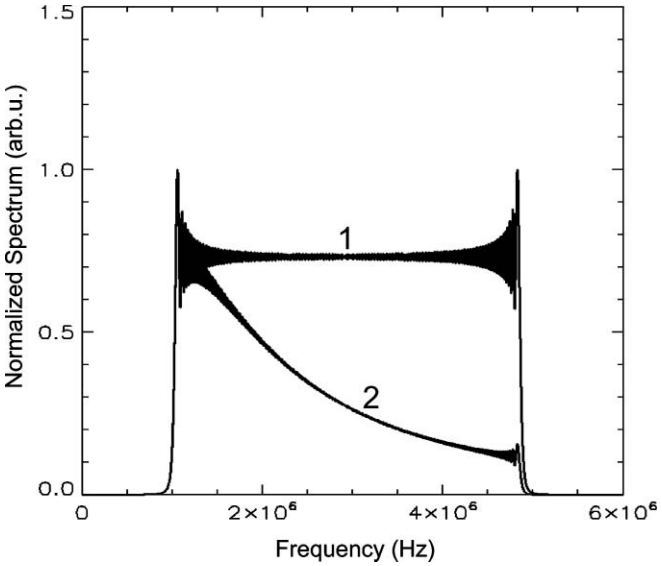

FIG. 3. Normalized spectrum of a chirped signal with frequency sweep 1–5 MHz and constant amplitude (curve 1) and the spectrum of a chirp weighted according to Eq. (7) with $\mu_a c_a = 1$ MHz (curve 2). Normalization was done with respect to maximum value.

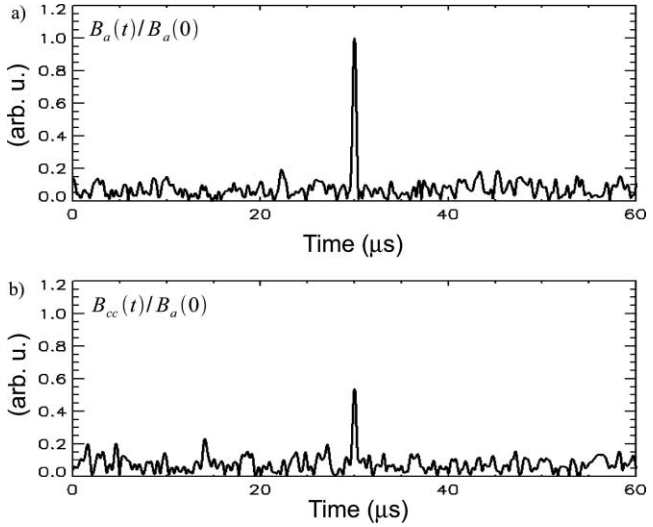

FIG. 4. Result of correlation processing of two chirps with the spectra shown in Fig. 3 and the input SNR = –40 dB. Normalized correlation function of a chirp with constant amplitude (a) and the chirp with spectrum weighted according to Eq. (7) (Fig. 3, curve 2) (b).

respect to the target chromophores and the detection instrumentation (primarily transducer transfer function). The actual SNR gain of the frequency-domain CW photoacoustics is usually lower than the time-bandwidth product for several reasons: nonuniformity of the transducer transfer function, frequency-dependent sound attenuation, and decrease of the PA pressure signal with increase of the modulation frequency as described by Eq. (7). The combined effect of these factors is a decrease of SNR gain with respect to the theoretical time-bandwidth product. The well-known decrease of the PA conversion efficiency with frequency[20] results in reduced contribution of the high-end frequency components of the chirp. The effect of the PA spectrum on the correlation function and on the SNR was investigated numerically using a delayed chirp with the spectrum transformed according to Eq. (7) and additive zero-mean Gaussian noise to simulate low-SNR measurements described by Eq. (10). The normalized spectrum of an ideal chirp with frequency sweep from 1 to 5 MHz is shown in Fig. 3 (curve 1). This chirp was delayed by 30 μs and Gaussian noise with standard deviation σ was added to produce SNR $= V_0^2/2\sigma^2 = -40$ dB. The result of correlation processing is shown in Fig. 4(a), which indicates the SNR gain close to that predicted theoretically by Eqs. (11) and (12). If we introduce photothermoacoustic frequency weighting as given by Eq. (7) with $\mu_a c_a = 1$ MHz, the chirp spectrum will be significantly compromised at the high-frequency end as shown in Fig. 3 (curve 2). Such transformation of the spectrum under otherwise identical conditions results in the reduction of SNR nearly by a factor of 2 [Fig. 4(b)]. Even with loss of the SNR inherent to PA conversion, the input chirped signal with SNR = –40 dB can be detected using correlation processing. An example of the correlation signal amplitude obtained using the experimental setup described earlier[14] for a planar absorber with $\mu_a = 2$ cm^{-1} immersed in tissuelike Intralipid solution 2 cm deep is shown in Fig. 5. These data were recorded using a focusing transducer (focal distance 5.08 cm and the peak frequency response at 0.5 MHz) with the absorber positioned near the focal zone. The chirp bandwidth was 600 kHz spanning the 200–800 kHz frequency range. Since the overall distance transducer–absorber included a layer of coupling water, the correlation peak was observed at 40 μs delay. Qualitative comparison with Fig. 1 for the pulsed response shows that the baseline interference was substantially less severe and the presence of signal can be easily detected, although the axial resolution is reduced due to low chirp bandwidth selected for this particular measurement.

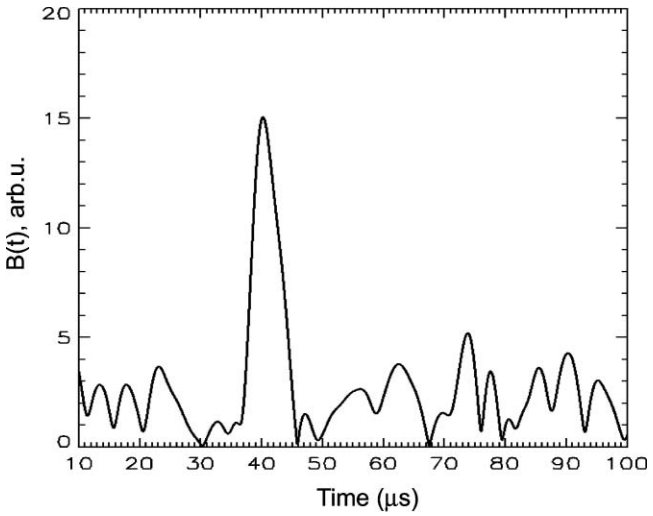

FIG. 5. Experimental correlation function of a chirped photoacoustic response received from a planar chromophore with $\mu_a = 2$ cm^{-1} immersed in tissuelike Intralipid solution 2 cm deep. Focusing transducer: 0.5 MHz and focus: 5.08 cm; chirp parameters: $\Delta f = 0.2$–0.8 MHz, $T_{ch} = 1$ ms.

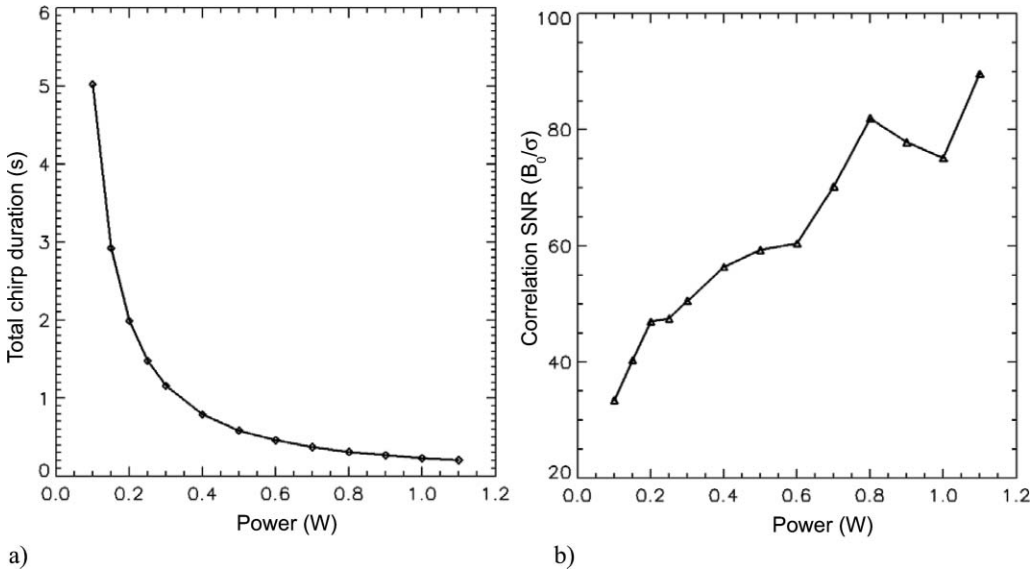

FIG. 6. Optimization of SNR in frequency-domain chirped photoacoustics with respect to laser power (laser spotsize = 2.8 mm) and chirp duration: (a) safe chirp duration for the given laser power and laser spotsize, (b) SNR as a ratio of correlation peak to noise standard deviation for the laser power and chirp duration varied according to the safety curve.

IV. OPTIMIZATION OF FREQUENCY-DOMAIN PHOTOACOUSTICS

To optimize the sensitivity of frequency-domain photoacoustics, important chirp parameters such as chirp central frequency, bandwidth, and duration must be carefully chosen by considering three factors: optical properties of the targeted chromophores, transducer transfer function, and laser power. The first two factors can be used to achieve optimal light-to-sound conversion and maximum response of the transducer. At the same time, the laser power (and irradiance) must be limited by the safety curve (Fig. 2), which in turn depends on chirp duration. The strong nonlinearity of the MPE curve versus exposure time carries an important implication for the signal-to-noise ratio and the trade-off between laser power and chirp duration. The standard expression for SNR of a matched filter can be written as[21]

$$\mathrm{SNR}_{\mathrm{MF}} = \frac{2E_s}{N_0} = \frac{A^2 T_{\mathrm{ch}}}{N_0}, \tag{13}$$

where E_s is the signal energy, A is the signal amplitude, T_{ch} is the chirp duration, and N_0 is the white noise power spectral density. It follows from Eq. (13) that both large signal amplitude $A \sim I_0$ and long chirp duration T_{ch} are beneficial to SNR. However, the laser irradiance I_0 must be related to T_{ch} according to the safety standard given by Eq. (9). Taking into account Eqs. (9) and (13), it is easy to show that for two laser chirps with I_{01} and I_{02} at the safety limit that have corresponding durations $\mathrm{T_{ch1}}$ and $\mathrm{T_{ch2}}$, the ratio of the two SNRs is

$$\frac{\mathrm{SNR}_2}{\mathrm{SNR}_1} = \left(\frac{T_{\mathrm{ch1}}}{T_{\mathrm{ch2}}}\right)^{1/2}. \tag{14}$$

Equation (14) shows that $\mathrm{SNR}_2 > \mathrm{SNR}_1$ if $T_{\mathrm{ch2}} < T_{\mathrm{ch1}}$. This result is somewhat unexpected from the standpoint of matched filter signal processing Eq. (13) and is entirely the result of safety requirements. Thus for the two examples depicted in Fig. 2, the one with irradiance 9 W/cm^2 and $T_{\mathrm{ch}} = 0.5$ s (straight line 1) is expected to have better SNR than the one with $I_0 = 4$ W/cm^2 and $T_{\mathrm{ch}} = 1.5$ s (line 2). Since the power of CW lasers is always limited, a simple prescription for maximizing SNR can be formulated as follows: the maximum available surface irradiance must be set first and then the chirp duration should be adjusted according to the safety curve. To demonstrate that SNR can be increased by increasing laser power and simultaneously shrinking chirp duration according to the safety curve $T_{\mathrm{ch}} \sim I^{-4/3}$ in terms of laser irradiance, we conducted experiments with a planar absorber immersed in a light-scattering Intralipid solution. Details of the experimental system were described in previous studies.[14] Results of the measurements are shown in Fig. 6. Figure 6(a) simply shows the safety curve for the maximum chirp duration T_{ch} corresponding to the chosen mean power and laser spotsize of 2.8 mm in diameter. For the purpose of this measurement, a fixed number N of shorter chirps with duration t_{ch} and the same bandwidth were averaged coherently while $T_{\mathrm{ch}} = N \times t_{\mathrm{ch}}$ was maintained. The SNR of the matched filter processing was measured as a ratio of the cross-correlation peak $B(0)$ to the standard deviation of noise floor σ. The result of SNR measurements for variable incident laser power and chirp duration adjusted according to Fig. 6(a) is shown in Fig. 6(b). These data indicate that SNR can be increased nearly by a factor of 3 by choosing higher laser power and shorter chirp duration, which is still lower than that predicted theoretically by Eq. (14) for $(T_{\mathrm{ch1}}/T_{\mathrm{ch2}})^{1/2} = 5$.

V. CONCLUSIONS

In this paper, we analyzed two photoacoustic modalities used for imaging biological tissues with respect to signal-to-noise ratios that can be achieved in typical PA experiments.

Optical parameters similar to those of human tissues and standard response characteristics of ultrasound sensors were utilized to estimate the laser-induced photoacoustic pressure and the voltage signal received by an ultrasonic transducer. Estimates of the SNR in both cases show that the pulsed time-domain technique offers higher SNR with respect to the thermal noise floor approximately by 10 dB but it is compromised with significant level of unwanted interference due to the broadband nature of signal detection. On the other hand, the photoacoustic method utilizing intensity-modulated CW lasers with chirped modulation waveforms can achieve similar (within order of magnitude) SNR performance with significantly less baseline interference and the same axial resolution. Major gain in SNR and submillimeter axial resolution can be achieved using correlation processing of a chirped photoacoustic response with high time-bandwidth product. It was shown that the laser safety standard requires particular attention to the laser power and chirp duration used for imaging human tissues. The SNR advantage of using shorter chirps with higher tissue irradiance was demonstrated experimentally. These results demonstrate that low-cost compact CW near-IR laser sources can be successfully used for high SNR and high contrast, spatially resolved photoacoustic imaging and provide reasonable alternative for the development of portable imaging instrumentation suitable for clinical applications.

ACKNOWLEDGMENTS

The authors gratefully acknowledge the support of the Natural Sciences and Engineering Research Council of Canada (NSERC) for Discovery and Strategic Grants, the Canada Research Chairs Program, and the Ontario Premier's Discovery Award in Science and Engineering to A.M., which made this research possible.

[1] S. Ermilov, T. Khamapirad, A. Conjusteau, M. Leonard, R. Lacewell, K. Mehta, T. Miller, and A. Oraevsky, J. Biomed. Opt. **14**, 024007 (2009).
[2] S. Manohar, A. Kharine, J. C. G. van Hespen, W. Steenbergen, and T. G. van Leeuwen, Phys. Med. Biol. **50**, 2543 (2005).
[3] J.-T. Oh, M.-L. Li, H. F. Zhang, K. Maslov, G. Stoica, and L. V. Wang, J. Biomed. Opt. **11**, 034032 (2006).
[4] D. Razansky, M. Distel, C. Vinegoni, R. Ma, N. Perrimon, R. W Köster, and V. Ntziachristos, Nature Photon. **3**, 412 (2009).
[5] J. Laufer, D. Delphy, C. Elwell, and P. Beard, Phys. Med. Biol. **52**, 141 (2007).
[6] X. Wang and L. V. Wang, *Photoacoustic Imaging and Spectroscopy*, edited by L. V. Wang (CRC Press, Boca Raton, 2009), p. 351.
[7] A. J. Welch and M. J. C. van Gemert, *Optical-Thermal Response of Laser Irradiated Tissue* (Plenum, New York, 1995).
[8] A. A. Karabutov, N. B. Podymova, and V. S. Letokhov, Appl. Phys. B **63**, 545 (1996).
[9] A. Oraevsky and A. Karabutov, Proc. SPIE **3916**, 228 (2000).
[10] A. A. Karabutov, E. V. Savateeva, N. B. Podymova, and A. Oraevsky, J. Appl. Phys. **87**, 2003 (2000).
[11] V. G. Andreev, A. A. Karabutov, and A. A. Oraevsky, IEEE Trans. Ultrason. Ferroelectr. Freq Control **50**, 1383 (2003).
[12] ANSI Z136. 1–2007, American National Standard for Safe use of Lasers, Laser Institute of America 2007.
[13] T. D. Khokhlova, I. M. Pelivanov, V. V. Kozhushko, A. N. Zharinov, V. S. Solomatin, and A. A. Karabutov, Appl. Opt. **46**, 262 (2007).
[14] S. Telenkov and A. Mandelis, J. Biomed. Opt. **14**, 044025 (2009).
[15] S. Telenkov and A. Mandelis, J. Biomed. Opt. **11**, 044006 (2006).
[16] S. Telenkov and A. Mandelis, J. Appl. Phys. **105**, 102029 (2009).
[17] V. E. Gusev and A. A. Karabutov, *Laser Optoacoustics* (AIP, Melville, New York, 1993).
[18] *Radar Handbook*, edited by M. I. Skolnik (McGraw-Hill, New York, 1990).
[19] B. Lashkari and A. Mandelis, Opt. Lett. **35**, 1623 (2010).
[20] Y. Fan, A. Mandelis, G. Spirou, and A. Vitkin, J. Acoust. Soc. Am. **116**, 3523 (2004).
[21] G. S. Kino, *Acoustic Waves: Devices, Imaging, and Analog Signal Processing* (Prentice-Hall, Englewood Cliffs, NJ, 1987).